Influence of Inclusion Characteristics on the Formability and Toughness Properties of a Hot-Rolled Deep-Drawing Quality Steel

S.K. Paul and A. Ray

In industrial practice, variations in the steelmaking process may cause significant change in inclusion characteristics. During hot rolling of flat steel products, manganese sulfides, which are plastic at elevated temperatures, are elongated in the rolling direction. These elongated inclusions affect the formability properties, such as ductility, strain hardening exponent, average plastic strain ratio, critical strain represented by the forming limit diagram, and Charpy V-notch (CVN) impact energy as well as fracture behavior.

The inclusion characteristics and microstructural features of three commercially produced hot-rolled deep-drawing quality steels were evaluated and their effects on formability and impact properties were investigated. All three heats were made in a basic oxygen furnace. Two heats were teemed into ingots while the other heat was argon purged and continuous cast. These heats were then processed into 3.10 mm thick strips with identical processing parameters.

Manganese sulfide stringers were found to reduce the transverse ductility, whereas yield and tensile strengths remained virtually the same in all directions. The formability parameters were not significantly affected by small variations in inclusion characteristics. However, CVN impact energy and impact transition temperature data were observed to improve with steel cleanliness. The sulfide stringers were also found to adversely affect the impact energy, transition temperature, and fracture behavior in the transverse direction.

Keywords

average plastic strain ratio, formability, forming limit diagram, impact energy, inclusions, strain hardening exponent

1. Introduction

THE INFLUENCE of nonmetallic inclusions on the mechanical behavior of steels has been widely studied (Ref 1-6). During hot rolling, the manganese sulfide (MnS) inclusions, which are plastic at elevated temperatures, become highly elongated in the rolling direction. These MnS-stringered inclusions drastically reduce the formability properties, such as ductility (Ref 7-9), stretchability (Ref 10, 11), and the critical strain (Ref 11, 12) at the onset of failure represented by the forming limit diagram (FLD) in the direction transverse to the rolling direction. The deleterious effect of such inclusions on formability properties can be minimized or even eliminated (Ref 11, 13) by sulfide shape control.

The Charpy V-notch (CVN) impact energy, which measures the toughness of steel, is intimately related to both the volume fraction and shape of the inclusions (Ref 2). The stringered inclusions markedly reduce the impact energy in the transverse direction (Ref 11, 14), giving rise to anisotropy. However, the effect of nonmetallic inclusions on impact transition temperature (ITT) is yet to be clearly established (Ref 13). Speich and Spitzig (Ref 8) have shown that transition temperatures are not affected by changes in the volume fraction or shape of sulfide inclusions. Kozasu et al. (Ref 3) have also found that the overall effect of elongated inclusions on transition temperature is insignificant. On the other hand, Pickering (Ref 15) has reported a noticeable effect of inclusions on ITT.

The present work was undertaken to elucidate the effect of inclusion characteristics on the formability and impact properties of commercially produced hot-rolled deep-drawing quality steels (used for forming low-pressure gas cylinders) with similar microstructural features.

S.K. Paul and **A. Ray**, Product Development Division, Research & Development Centre for Iron & Steel, Steel Authority of India Limited, Ranchi - 834002, India.

2. Experimental Procedure

Three commercial heats were made in a basic oxygen furnace of 130 ton capacity. The purity of oxygen blown was 99.5% for all the heats. The required amounts of silico-manganese (Si-Mn), ferro-silicon (FeSi), lime, and aluminum were added in the ladle during tapping to deoxidize the steel and to achieve the desired compositions. Heats A and C were teemed into ingots of 22.5 tons each and subsequently rolled into slabs 200 mm thick and 1300 mm wide. Heat B was subjected to argon stirring for 5 min and then continuous cast into slabs 200 mm × 1300 mm in cross section. The chemical compositions of the three heats are shown in Table 1. The slabs of all these heats

Table 1 Chemical composition of the steels investigated

	Composition, wt %					
Heat	C	Mn	P	S	Si	Al
A	0.10	0.44	0.014	0.024	0.05	0.03
B	0.09	0.42	0.021	0.018	0.16	0.05
C	0 11	0.46	0 016	0.025	0.07	0.04

were hot rolled in a hot-strip mill to 3.1 mm thick coils. During hot rolling, the finishing and coiling temperatures were maintained in the range of 880 to 900 °C and 670 to 700 °C, respectively. These coils were then trimmed and sheared into sheets 3.15 × 1250 × 2500 mm. Full-width (1250 mm) samples were collected from the middle of the coils for the present investigation.

Specimens were prepared for the evaluation of various microstructural and mechanical properties from the half-width position of each strip sample. The morphology of inclusions and microstructures of the steels were examined in the longitudinal through-thickness direction. For observation of inclusions, the steel samples were hardened by austenitizing at 900 °C for half an hour, followed by oil quenching to prevent any pullout of the inclusions during polishing. These hardened samples were then polished to the stipulated metallographic finish by using diamond paste. The average grain diameters were measured from the micrographs using the linear intercept method, and the corresponding ASTM grain sizes were determined from the standard tables. The volume fractions of pearlite and nonmetallic inclusions were determined using a quantitative image analyzer. The analyses of inclusions were carried out in a computer-controlled electron-probe microanalyzer, JEOL JCXA-733 (JEOL Ltd., Akishima, Tokyo). For quantitative analysis of oxide inclusions, oxide standards were used and the raw x-ray intensity data were corrected by a ZAF program (PACX) supplied by JEOL.

The tensile properties were evaluated in three directions (longitudinal, transverse, and 45° to the rolling direction) on a 10 ton static universal testing machine, INSTRON-1195 (Instron Ltd., High Wycombe, Bucks, UK) at a crosshead speed of 5 mm/min. The tensile specimens were of 50 mm gage length and 12.5 mm width and were ground finished. During tensile testing, a 50 mm extensometer was used until fracture to measure the uniform and total elongations. True stress (σ) and the corresponding true strain (ε) values were calculated at several points within the region of uniform elongation. The strain hardening coefficient (n) was computed using Hollomon's equation ($\sigma = k\,\varepsilon^n$ where k is the strength coefficient). The n values corresponding to tensile axis inclined at 0°, 45°, and 90° to the rolling direction were determined, and the average strain hardening exponent ($\bar{n}$) values were calculated from the relation $\bar{n} = (n_0 + n_{90} + 2n_{45})/4$.

The average plastic strain ratios ($\bar{r}$) and planar anisotropy (Δr) values of these steels were measured following the procedure described by Keeler (Ref 16). The FLDs were evaluated in the transverse direction using a universal sheet and strip metal testing machine, Erichsen 145-60 (Erichsen, Hemer-Sundwig, Germany). The specimens used were 220 mm long and had widths varying in the range of 25 to 200 mm (in multiples of 25 mm). The samples were ground to 2.8 mm from the original sheet thickness of 3.10 mm. These specimens were electrochemically grid marked with 5 mm diameter contacting-type circular grids, then punch stretched to failure without load interruption using a 100 mm diameter hemispherical punch. The methodology used for evaluation of FLD has been reported by Paul et al. (Ref 17). The deformation speed during stretching was kept constant at 12 mm/min. Two blanks were tested for each width to obtain more data points.

The CVN impact energy was evaluated for quarter-size specimens (10 × 2.5 × 55 mm) at various temperatures from ambient (28 °C) to −80 °C in both the longitudinal and transverse directions. The fracture surfaces of both the tensile- and impact-tested specimens were examined in a scanning electron microscope (SEM).

Table 2 Microstructural features of the steels investigated

Heat	Pearlite, vol%	Grain size	
		Average diameter, μm	ASTM No.
A	11.37	14.35	9-10
B	10.26	15.20	9-10
C	11.40	13.15	9-10

Table 3 Inclusion characteristics of the steels investigated

Heat	Inclusions, vol%	Type of inclusions
A	0.46	Mostly MnS stringers. Oxides (Al_2O_3) usually enveloped by MnS, were also observed.
B	0.30	Mostly Al_2O_3 stringers. A few MnS stringers were also visible.
C	0 40	Mainly MnS stringers. Oxides (Al_2O_3), either isolated or enveloped by MnS, were also noticed.

3. Results and Discussion

3.1 *Microstructure*

The microstructures of the three steels showed fully recrystallized ferrite and pearlite grains, typical of a normalized steel (Fig. 1). The microstructures were also found to be homogeneous from surface to center. Such microstructures were achieved by controlling the finishing and coiling temperatures, as mentioned earlier. The volume fractions of pearlite, the average grain diameters, and the corresponding ASTM grain sizes of these steels are shown in Table 2. These microstructural features were found to be similar, due to the fact that the chemical compositions (Table 1) and the hot-rolling parameters of all the steels were identical.

3.2 *Inclusion Characteristics*

The inclusion characteristics of all three steels are shown in Table 3. The inclusions observed comprised mainly sulfides and oxides, as shown in Fig. 2. In heat A, the inclusions were mainly manganese sulfide stringers, although some oxides usually enveloped by sulfides, were also observed. In heat B, oxide inclusions, either distributed randomly or in the form of stringers, were found to be predominant. However, some tiny sulfide stringers were also occasionally observed. In heat C, the inclusions were again mainly MnS stringers, but oxides (either isolated or enveloped by sulfides) were also noticed. The volume fractions of inclusions (both oxides and sulfides together) as determined by image analysis are shown in Table 3. Heat B, subjected to argon purging, was found to be the cleanest of all heats and contained 0.30% volume fraction of inclusions. Heat

C, with 0.40% volume fraction of inclusions, was marginally cleaner than heat A, although both steels had a similar type of inclusions.

Electron-probe microanalysis of inclusions revealed that the sulfides were pure MnS in all the steels. The oxide inclusions were found to be mainly pure Al_2O_3 (Fig. 3). In some cases, however, alumina-rich galaxite ($MnO \cdot Al_2O_3$) containing up to 10% MnO was also observed. No silicon was detected in these oxide inclusions, even for heat B, which contained 0.16% Si (Table 1). The addition of manganese and aluminum together in the ladle during tapping can lead to the formation of spinel of varying compositions. Manganese enters into deoxidation reactions and forms galaxites (Ref 18), which enhances the deoxidizing power of aluminum

3.3 *Tensile Properties*

The room-temperature tensile properties of the three steels in different directions are shown in Table 4. Almost identical tensile properties were obtained in the rolling direction and 45°

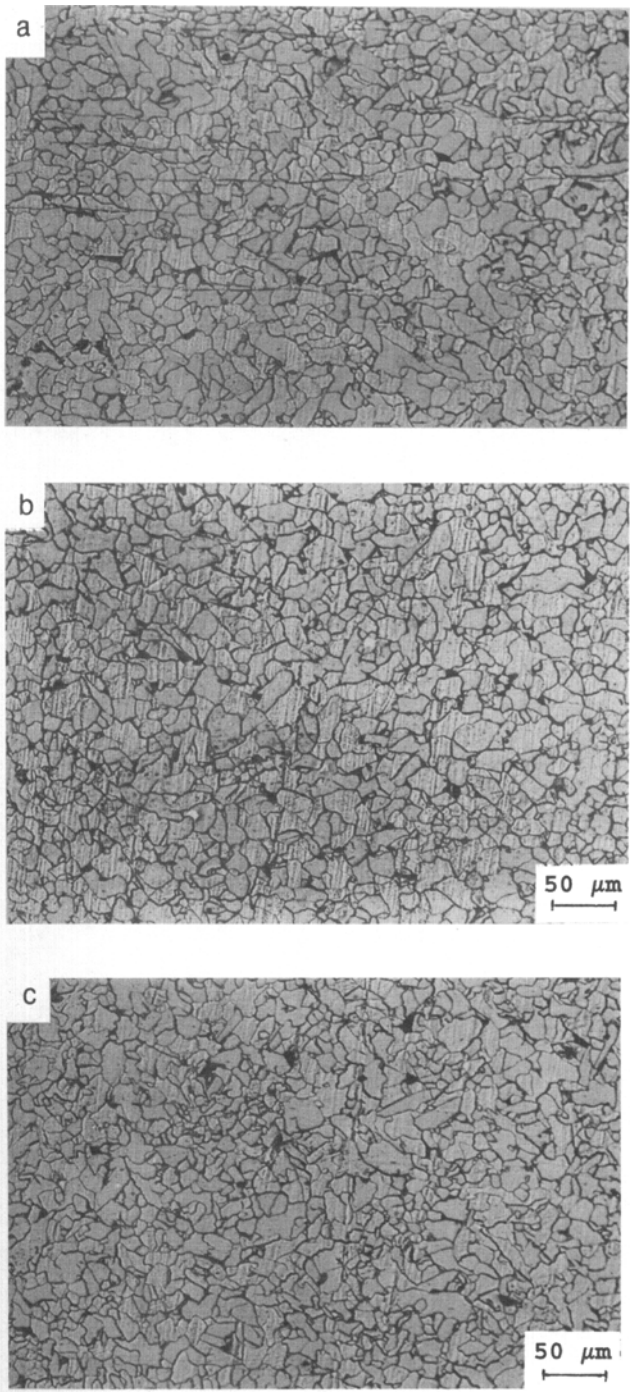

Fig. 1 Microstructures of steels showing recrystallized ferrite and pearlite grains. (a) Heat A. (b) Heat B. (c) Heat C

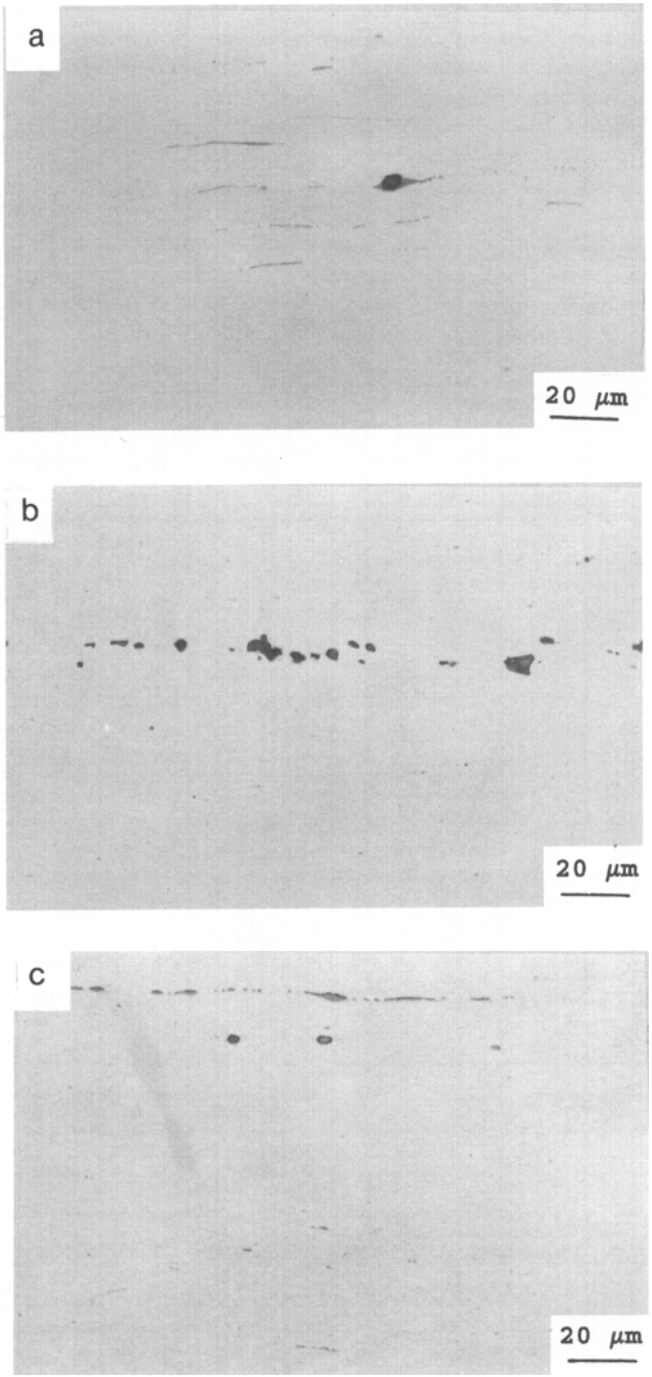

Fig. 2 Typical inclusions observed in different heats. (a) Heat A. (b) Heat B. (c) Heat C

to the rolling direction of each heat. However, the uniform and total elongations in the transverse direction were found to be slightly lower than the corresponding longitudinal values due to the presence of elongated sulfide inclusions. The yield and tensile strengths remained largely unaffected. Other research (Ref 7, 8, 14) has also shown that MnS stringers reduce the ductility in the transverse direction and that the influence is dependent on the strength level of the steel (the higher the strength, the lower the ductility). The tensile ductility also depends on the steel cleanliness (Ref 6) as well as the size and chemistry of inclusions (Ref 5). Heat B, despite being the cleanest of the steels (Table 3), showed lowest elongations in all directions (Table 4). This is because of the different inclusion characteristics of heat B, which contained mostly Al_2O_3 inclusions, often as stringers. With similar inclusion characteristics, heats A and C showed almost identical uniform and total elongations in all directions (Table 4).

The fracture surface of broken transverse tensile specimens revealed two sets of voids (Fig. 4): large voids, which were nucleated at inclusions, and smaller voids in between the large voids. Others (Ref 7, 9) have reported similar fracture appearances. According to Kozasu and Kubota (Ref 7), the first event in the formation of voids during tensile deformation is the cracking of sulfide inclusions and the decohesion of the inclusion-matrix interface. These cracks grow in size during plastic deformation and finally attain a dimension and shape comparable to that of the nucleating inclusion. The final separation proceeds by microvoid formation from submicron particles and their coalescence, resulting in a dimple pattern on the fracture surface, as evident from Fig. 4. Heats A and C, with longer MnS stringers, showed larger voids than heat B, which showed tiny MnS inclusions inside the smaller voids.

3.4 *Formability Properties*

The formability of sheet steel in stamping operation primarily depends on the average strain hardening exponent ($\bar{n}$), average plastic strain ratio ($\bar{r}$), and the maximum strain the material can undergo before the onset of localized necking (Ref 11). The strain hardening exponent measures the ability of the material to distribute strain uniformly, and the steel with a high $\bar{n}$ value exhibits good stretching behavior. The n values in different directions and the $\bar{n}$ values of each steel investigated are shown in Tables 4 and 5, respectively. The n values were found to be identical in the longitudinal direction and 45° to the longitudinal direction for each steel (Table 4). It has been shown (Ref

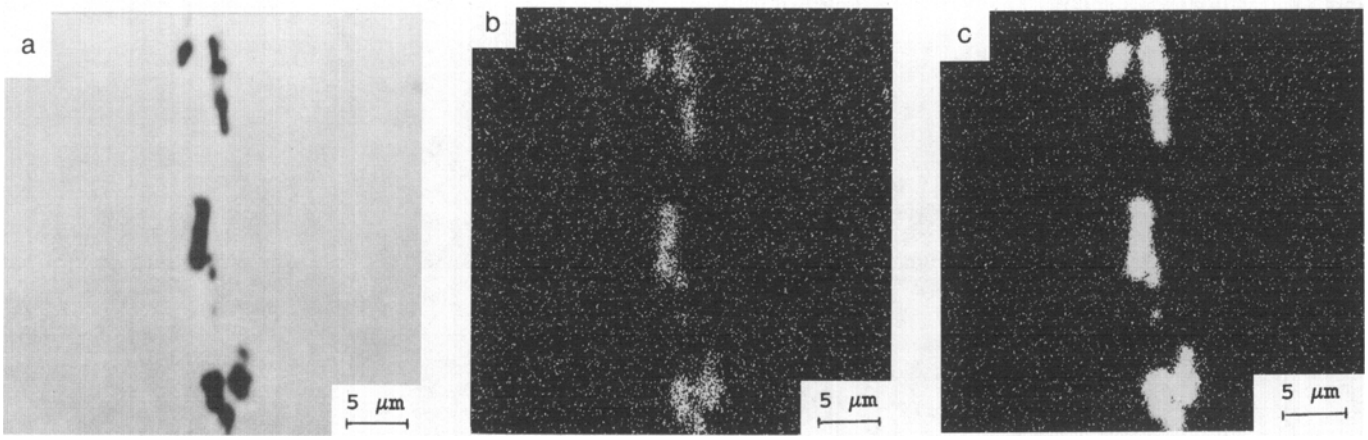

Fig. 3 Electron-probe microanalysis scans of Al_2O_3 inclusions observed in heat B. (a) Backscattered electron image. (b) Oxygen x-ray map. (c) Aluminum x-ray map

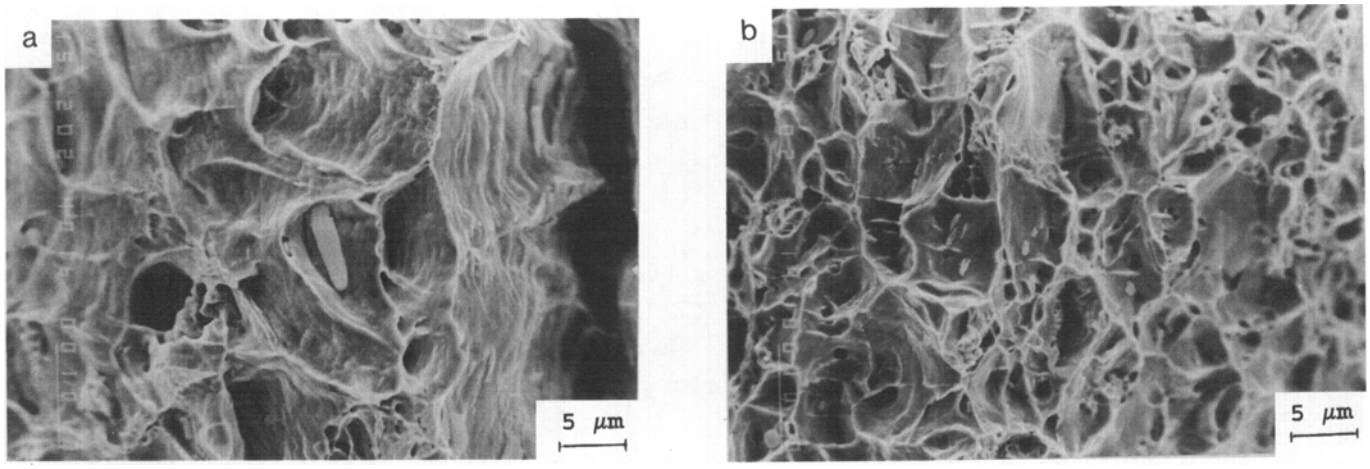

Fig. 4 SEM fractographs of tensile-tested specimens in the transverse direction. (a) Heat A. (b) Heat B

11) that sulfide stringers reduce the n value more in the transverse direction than in the rolling direction. This is also reflected in the present work for all the steels. However, the difference between n values in the longitudinal and transverse directions is less in steel B than in the other two steels (Table 4). This could be attributed to the presence of fewer sulfide stringers in that steel. The $\bar{n}$ values were found in the range of 0.204 to 0.210 (Table 5), which are normal for hot-rolled deep-drawing quality steels. Heat B showed the lowest $\bar{n}$ value (0.204) despite being the cleanest of all three steels (Table 3). The various important factors which affect the $\bar{n}$ value are grain size, alloying elements, and the presence of second-phase particles (Ref 19). The higher silicon content (Table 1) and more alumina inclusions in heat B resulted in the lowest $\bar{n}$ value since grain sizes were similar for all the steels.

The Erichsen cup heights at failure were also measured for the three steels and are shown in Table 5. The Erichsen cup value (E_V) basically reflects the stretchability of the material and is directly related to the strain hardening exponent. The E_V values were found to be in the range of 16.2 to 16.5 mm. Heat B, with the lowest $\bar{n}$ value, showed the minimum Erichsen cup height at failure.

The average plastic strain ratios ($\bar{r}$) and the planar anisotropy values (Δr) of all the steels are given in Table 5. The $\bar{r}$, which is an index of the depth of drawing, is dependent on the crystallographic texture (Ref 20). The $\bar{r}$ values obtained for all the steels were low (0.90 to 0.96). Others (Ref 11, 21) have also reported low $\bar{r}$ values for hot-rolled steels because of the weak crystallographic texture. Although the highest $\bar{r}$ value (0.96) was obtained for the cleanest steel (heat B), the variations observed in $\bar{r}$ for the steels investigated is quite normal for regular commercial production. It has also been shown (Ref 11) that the cleanliness or the type of inclusions present in the steel does not significantly affect the $\bar{r}$ value. The Δr values of all the

Table 4 Tensile properties of the steels investigated

Heat	Direction(a)	Yield strength, kg/mm²	Tensile stregth, kg/mm²	Uniform elongation (GL=50 mm), %	Total elongation (GL=50 mm), %	Strain hardening exponent (n)
A	L	25.82	36.81	23.4	36.2	0.210
	T	26.15	37.25	22.5	34.3	0.203
	X	25.94	36.95	23.6	37.0	0.212
B	L	27.71	39.41	22.8	35.4	0.205
	T	29.32	39.84	22.2	33.2	0.200
	X	28.43	39.02	22.8	35.0	0.205
C	L	28.12	40.82	23.6	36.3	0.212
	T	28.31	40.56	22.6	34.5	0.203
	X	28.50	41.12	23.8	37.3	0.213

L, Longitudinal, T, Transverse; X, 45° to the longitudinal direction; GL, gauge length

Table 5 Formability properties of the steels investigated

Heat	E_v, mm	$\bar{n}$	$\bar{r}$	Δr	FLD_0, %
A	16.4	0.209	0.90	–0.13	51.5
B	16.2	0.204	0.96	–0.21	51.0
C	16.5	0.210	0.92	–0.14	52.0

Table 6 Charpy V-notch impact energies of the steels investigated

Temperature, °C	CVN impact energy (kg · m/cm²)					
	Heat A		Heat B		Heat C	
	L	T	L	T	L	T
28	12.81	7.26	16.61	9.43	12.64	7.57
0	12.09	6.88	16.22	9.23	11.96	7.35
–15	11.32	6.74	16.06	9.22	11.76	7.26
–30	10.87	6.36	15.78	8.88	11.47	6.86
–45	9.00	5.48	15.58	8.56	10.66	6.33
–50	...	5.25	. .	...	...	...
–60	7.96	0.99	15.49	7.57	8.41	5.14
–65	7.53	...	...	..	...	1.24
–70	0.75	...	...	...	...	...
–75	0.33	0.33	14.43	6.09	7.51	0.70
–80	...	...	...	2.50	...	...

L, Longitudinal direction; T, Transverse direction

steels were negative (Table 5), which shows that the favorable texture is stronger in the 45° orientation than in the 0° and 90° orientations. This also indicates that the formation of ears will occur at 45° to the rolling direction. Heat B, with maximum $\bar{r}$, showed highest Δr, which is in agreement with other (Ref 16) research.

The FLDs, which represent the critical strain (Ref 17) at the onset of failure, were evaluated in the transverse direction for all three heats. Figure 5 shows the FLD of heat C. The level of FLD, as measured by the plane-strain intercept, (FLD_0) was found to be in the range of 51 to 52% (Table 5). The shape and level of FLDs were found to be very similar for all these steels. While the level of FLD is largely controlled by average strain hardening exponent and sheet thickness (Ref 17), the presence of large elongated inclusions can result in premature fracture, thereby lowering the results (Ref 22). However, in the present study, the adverse effect of sulfide stringers has not been observed. On the other hand, heat B, with fewer sulfide stringers, showed marginally lower FLD_0 than heats A and C, which can be attributed to its lower $\bar{n}$ value.

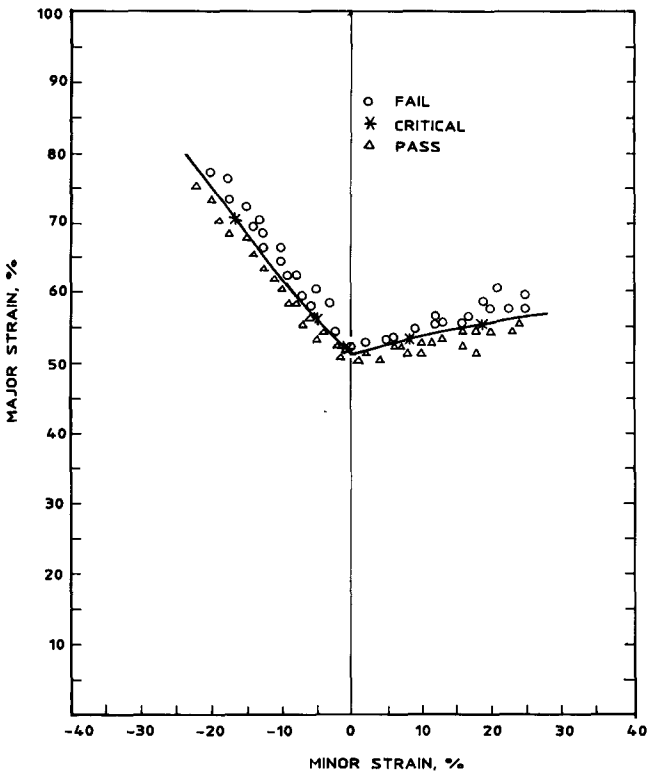

Fig. 5 Forming limit diagram of heat C

3.5 *Impact Properties*

The CVN impact energies of all three heats at various temperatures are listed in Table 6. Each data point in the table is the average of the five best matching values obtained for that particular set. The CVN impact curves for longitudinal and transverse specimens are shown in Fig. 6, 7, and 8 for heats A, B, and C, respectively. It can be seen from these figures that inclusion content has a marked effect on the upper-shelf energy. Heat B, being cleanest, showed higher impact values than heats A and C at all test temperatures. Elongated sulfide inclusions have a

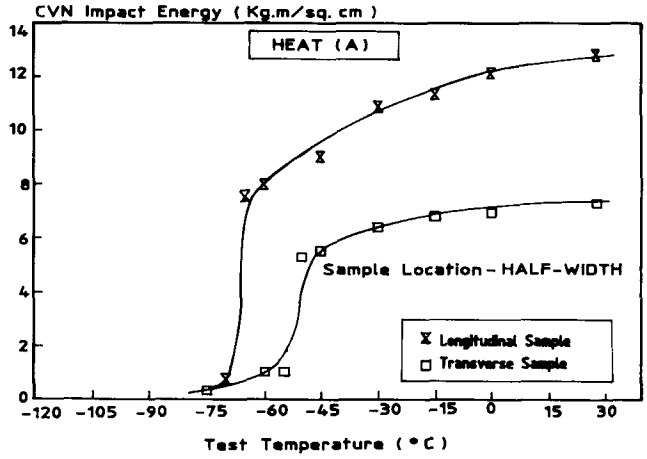

Fig. 6 Variation of CVN impact energy (in kg·m/cm^2) with temperature for heat A

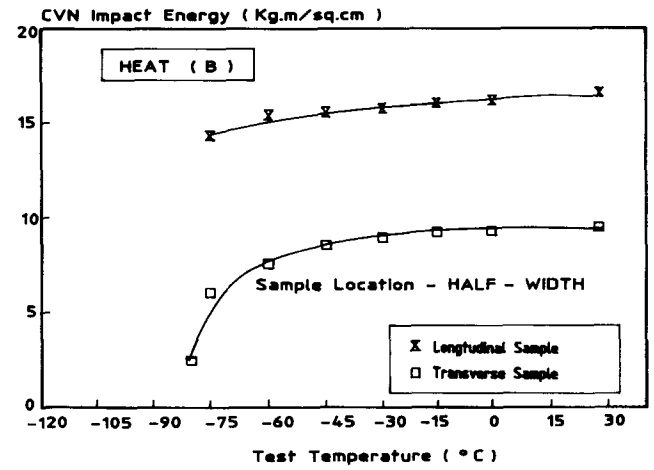

Fig. 7 Variation of CVN impact energy (in kg·m/cm^2) with temperature for heat B

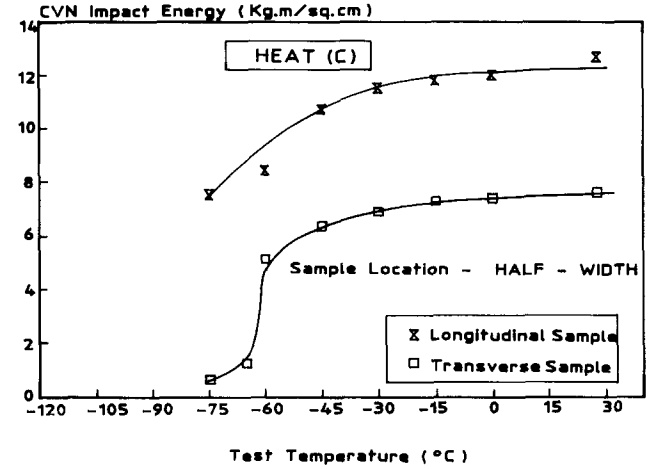

Fig. 8 Variation of CVN impact energy (in kg·m/cm^2) with temperature for heat C

pronounced effect in decreasing the impact energy in the transverse direction (Ref 3, 11, 14). This effect is also noticeable in the present study, where all three heats showed much lower impact energy values in the transverse direction than in the longitudinal direction. Heat B, with fewer MnS stringers, exhibited higher impact energy values in the transverse direction, as shown in Fig. 9. The anisotropy in impact properties (ratio of transverse to longitudinal impact energy values) of all three heats are depicted in Table 7 at various test temperatures. Similar impact energy ratios (0.57 to 0.60) were observed for all the heats at ambient temperature (28 °C). The anisotropy was found to be maximum (0.10 to 0.12) in the vicinity of impact transition temperature (ITT).

The ITTs for transverse specimens were higher than for corresponding longitudinal specimens in each heat (Fig. 6-8). This could be attributed to the larger area fraction of sulfide stringers in the transverse direction. Some investigators (Ref 3, 8) have shown that the elongated sulfide inclusions do not adversely affect the transition temperature of lower-strength steels, but in the present study the effect of sulfide stringers was observed to increase the ITT in transverse directions (Fig. 6-8). Spitzig et al. (Ref 2) have also reported higher ITT in the transverse direction. The effect of steel cleanliness as measured by volume fraction of inclusions can be seen from Fig. 9, which shows the CVN impact energy curves in the transverse direction for all the heats. It is evident from the figure that ITT decreased with increasing steel cleanliness. Heat A, with more volume fraction of inclusions (Table 3), showed higher ITT. The much lower ITT in heat B could be attributed to the combined effect of greater cleanliness and lower incidence of elongated sulfide inclusions. The other factors which affect the ITT of steel are chemistry, grain size, pearlite content, and strength level. Since all these parameters were similar for the three steels investigated, the variation observed in ITT may be attributed to the inclusion characteristics only.

The fracture surfaces of transverse impact specimens were examined in a SEM. It was observed that at room temperature, the fracture occurred by completely ductile mode with void nucleation and growth at inclusions, followed by localized shear between these voids (Fig. 10). Heats A and C, containing more MnS stringers, showed greater area fraction of large inclusion-nucleated voids on the fracture surface as compared to heat B. With decrease in test temperature, the mode of fracture was found to change from ductile to quasicleavage and finally to total cleavage failure at ITT and below. The fractograph at –45 °C for heat A (Fig. 11) clearly shows a quasicleavage fracture with tear ridges separating cleavage facets.

Table 7 CVN impact energy ratios (transverse to longitudinal) of the steels investigated

Temperature, °C	Impact energy ratio		
	A	B	C
28	0.57	0.57	0.60
0	0.57	0.57	0.61
–15	0.59	0.57	0.62
–30	0.58	0.56	0.60
–45	0.61	0.55	0.60
–60	0.12	0.49	0.61
–75	1.00	0.42	0.10

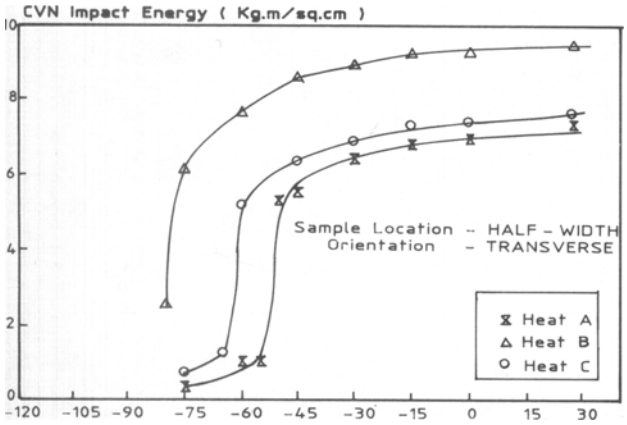

Fig. 9 Composite plot showing variation of CVN impact energy (in kg·m/cm^2) with temperature for transverse specimens of heats A, B, and C

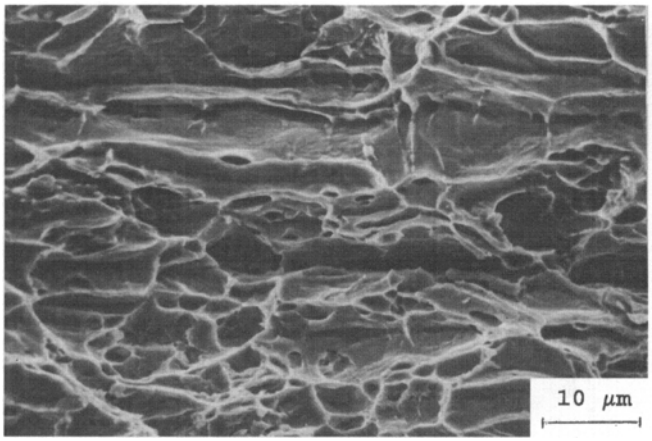

Fig. 10 SEM fractograph of impact-tested specimen showing ductile fracture at 28 °C (heat A)

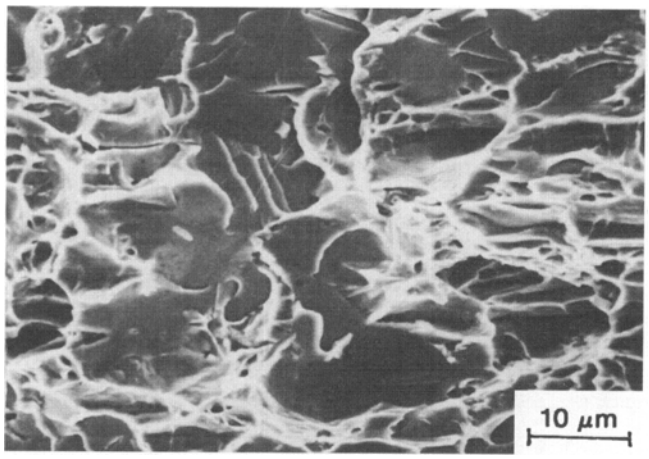

Fig. 11 SEM fractograph of impact-tested specimen showing quasicleavage fracture at –45 °C (heat A)

4. Summary and Conclusions

- Elongated MnS stringers were found to reduce total elongation in the transverse direction by 2 to 3%, whereas yield and tensile strengths remained largely unaffected. The tensile properties were found to be almost identical in the longitudinal direction and 45° to the longitudinal direction in each steel.
- The formability parameters ($\bar{r}$ and $\bar{n}$) and FLDs were not significantly affected by small variations in inclusion characteristics under industrial practice. The n values were found to be marginally lower in the transverse direction than in the longitudinal direction. The level of FLD was found to be dependent more on the average strain hardening exponent ($\bar{n}$) than the volume fraction or type of inclusions present in the steel. Heat B, with less volume fraction of inclusions, showed lower level of FLD because of minimum $\bar{n}$ value.
- CVN impact energy was found to be greater in cleaner steel. Heat B, containing 0.30% volume fraction of inclusions, showed about 1.3 times higher CVN impact energy values than heats A and C, which contained 0.46 and 0.40% volume fractions of inclusions, respectively.
- Elongated inclusions were found to drastically reduce the CVN impact energy in the transverse direction. Despite fewer MnS stringers in heat B, the anisotropy ratio (0.57) was found to be similar to that in the other two heats due to the presence of a large number of Al_2O_3 stringers.
- ITT was found to be dependent on steel cleanliness. Heat B, with the lowest volume fraction of inclusions, showed the lowest ITT in both directions.
- The sulfide stringers were found to more adversely affect the ITT in the transverse direction than in the longitudinal direction in each heat. The ITT in heat B was significantly lower in the transverse direction than in the other two heats due to the presence of fewer MnS stringers.

Acknowledgments

The authors are grateful to the management of R&D Centre, Steel Authority of India Limited, Ranchi for their encouragement and support. The help rendered by the laboratory technicians in the metallography and mechanical testing laboratories is also sincerely acknowledged.

References

1. A.J. Birkle, R.P. Wei, and G.F. Pellissier, *Trans. ASM,* Vol 54, 1966, p 981
2. W.A. Spitzig and R.J. Sober, *Metall. Trans. A,* Vol 12 (No. 2), 1981, p 281
3. I. Kozasu, T. Shimizu, and H. Kubota, *Trans. ISIJ,* Vol 13 (No. 1), 1973, p 20
4. T. Gladman, B. Holmes, and I.D. McIvor, "Effect of Second Phase Particles on the Mechanical Properties of Steel," Special Report 145, Iron and Steel Institute, London, 1971, p 68
5. S.K. Paul, A.K. Chakrabarty, and S. Basu, *Trans. IIM,* Vol 39 (No. 3), 1986, p 219
6. S.K. Paul, A.K. Chakrabarty, and S. Basu, *Metall. Trans. B,* Vol 13, 1982, p 185
7. I. Kozasu and H. Kubota, *Trans. ISIJ,* Vol 11 (No. 5), 1971, p 321
8. G.R. Speich and W.A. Spitzig, *Metall. Trans. A,* Vol 13 (No. 12), 1982, p 2239
9. W.A. Spitzig, *Metall. Trans. A,* Vol 14, 1983, p 471
10. S.P. Keeler and W.G. Brazier, "Micro Alloying 75, Union Carbide Corp., p 517
11. S.K. Paul and S. Mishra, *Metals Materials and Processes,* Vol 4, 1992, p 189
12. A. Nicholson and T. Gladman, *Ironmaking and Steelmaking,* Vol 13, 1986, p 53
13. A. Ray, S.K. Paul, and S. Jha, *J. Mater. Eng. Perform.,* Vol 4 (No. 6), 1995, p 679
14. L. Luyckx, J.R. Bell, A. McLean, and M. Korchynsky, *Metall. Trans.,* Vol 1, 1970, p 3341
15. F.B. Pickering, in *Proc. Symp. Toward Improved Ductility and Toughness,* Climax Molybdenum Development Co., 1971, p 9
16. S.P. Keeler, Understanding Sheet Metal Formability, paper presented to St. Louis Chapter, American Society for Metals, Nov 1972
17. S.K. Paul, S. Kumar, S. Mishra, and V. Ramaswamy, *Trans. IIM,* Vol 45, 1992, p 163
18. E. Plockinger, "Clean Steel 64," Iron and Steel Institute, London, 1963
19. W.B. Morrison, *Trans. ASM,* Vol 50, 1966, p 824
20. S. Mishra and C. Darmann, *Int. Metals Reviews,* Vol 27, 1982, p 307
21. R.L. Whiteley and D.E. Wise, *Flat Products III,* AIME, 1962, p 47
22. J. Hiam and A. Lee, *Sheet Met. Ind.,* Vol 55, 1978, p 631